Design and implementation of a full profile sub-cm ruby laser based Thomson scattering system for MAST

T. O'Gorman,[1] P. J. Mc Carthy,[1] S. Prunty,[1] M. J. Walsh,[2,a)] M. R. Dunstan,[2] R. B. Huxford,[2] G. Naylor,[2] Emmanuel Maguet,[2] R. Scannell,[2] and S. Shibaev[2]
[1]*Department of Physics, University College Cork, Association Euratom-DCU, Cork, Ireland*
[2]*EURATOM/CCFE Fusion Association, Culham Science Centre, Abingdon, Oxfordshire, OX14 3DB, United Kingdom*

(Received 11 May 2010; accepted 11 October 2010; published online 22 December 2010)

A major upgrade to the ruby Thomson scattering (TS) system has been designed and implemented on the Mega-ampere spherical tokamak (MAST). MAST is equipped with two TS systems, a Nd:YAG laser system and a ruby laser system. Apart from common collection optics each system provides independent measurements of the electron temperature and density profile. This paper focuses on the recent upgrades to the ruby TS system. The upgraded ruby TS system measures 512 points across the major radius of the MAST vessel. The ruby laser can deliver one 10 J 40 ns pulse at 1 Hz or two 5 J pulses separated by 100–800 μs. The Thomson scattered light is collected at F/15 over 1.4 m. This system can resolve small (7 mm) structures at 200 points in both the electron temperature and density channels at high optical contrast; ~50% modulated transfer function. The system is fully automated for each MAST discharge and requires little adjustment. The estimated measurement error for a 7 mm radial point is <4% of T_e and <3% of n_e in the range of 40 eV to 2 keV, for a density of $n_e = 2 \times 10^{19}$ m^{-3}. The photon statistics at lower density can be increased by binning in the radial direction as desired. A new intensified CCD camera design allows the ruby TS system to take two snapshots separated with a minimum time of 230 μs. This is exploited to measure two density and temperature profiles or to measure the plasma background light. © *2010 American Institute of Physics*. [doi:10.1063/1.3511556]

I. INTRODUCTION

One of the challenges of plasma physics diagnostics is achieving greater spatial and temporal resolution measurements of the H-mode pedestal, edge localized modes, magnetic islands, internal transport barriers, and other phenomena related to plasma evolution and transport. The ruby Thomson scattering (TS) system has been redesigned and upgraded to probe sub centimeter spatial scales in MAST. Measurement on these scales are required in particular to study the width of the H-mode pedestal (1–2 cm on MAST) and the seed island physics of Neoclassical tearing modes (NTMs). The flattening of the temperature profile for the onset of a NTM on MAST is predicted to be of the order of ~1 cm.

A new 512 point dual snapshot TS system has been designed to replace the previous one described in Refs. 1 and 2. This system is a CCD based TS system (TVTS), as detailed in Refs. 3–5, and has a spatial resolution of ~7 mm. Although existing systems have been designed to measure sub centemeter radial resolution, one of the novelties of this upgraded system is that high radial resolution is maintained over a large 1.4 m laser chord. The effective number of points this system can resolve ~200 at high 50% modulated transfer function (MTF) is greater than similar TVTS systems. In this paper, the contribution each component makes to the resolution is presented.

The upgraded system has also increased the number of scattered photons detected by a factor of ~3 compared to the previous system, by replacing the previous GaAs image intensifier with a filmless GaAsP image intensifier that has a greater effective quantum efficiency (EQE). In addition, a new Princeton Instruments ProEM frame transfer CCD camera has been utilized with a custom-designed triggering unit to allow the system to measure the background plasma light or operate in double pulse mode.

In Fig. 1 the schematic layout of the complete ruby TS system is shown. Light from a Q switched ruby laser is injected into the plasma along the mid-plane of the MAST. An F/6 collection lens collects the scattered light from a 1.4 m laser chord between scattering angles of 83–120 degrees. This is imaged onto 85 fiber bundles; each bundle is 4.95 mm × 1.82 mm and collects scattering light at F/1.75. The light is transported 12 m along the fibers to the ruby spectrometer.

At the spectrometer the bundles are arranged to form an 8.5 mm × 130 mm input slit. Although the spectrometer is designed to have a high optical throughput, in this type of system etendue is limited by the diameter of the image intensifier and also the required spectral resolution, which sets the width of the input slit. Spectral resolution is required primarily for removal of the laser line and the D-alpha line at the field mirror. A relay lens system collects F/4 of the F/1.75 light cone delivered, dropping the effective F/# number of the collection lens to F/15. The fiber bundles have also been designed to allow for the spectrometer system to be upgraded to collect all scattered light from the collection lens.

After the relay lens system, light from the fiber bundles is guided onto two holographic notch filters using a telecentric lens system. The light then passes through a Littrow lens,

[a)]Present address: ITER Organisation, Diagnostics Division, CHD Department, Cadarache, France.

 © 2010 American Institute of Physics

Downloaded 11 Aug 2011 to 194.81.223.66. Redistribution subject to AIP license or copyright; see http://rsi.aip.org/about/rights_and_permissions

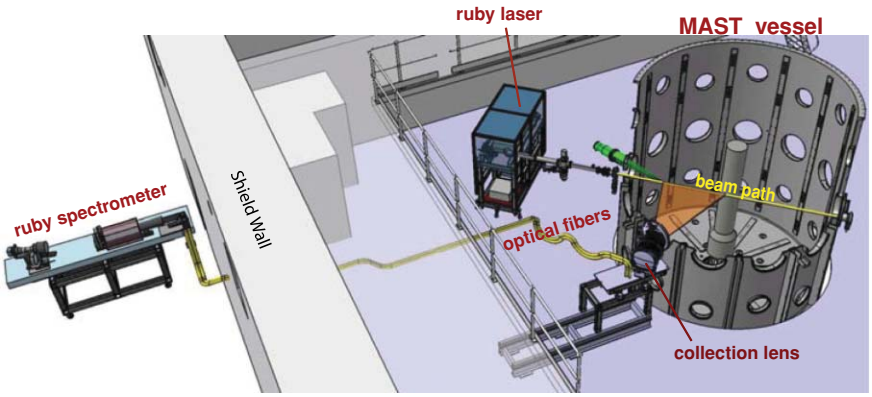

FIG. 1. (Color online) Layout of the ruby TS system on MAST.

grating and spherical field mirror onto an F/0.7 image intensifier lens. A GaAsP Gen 3 filmless image intensifier is contact mounted to this lens system. The light from the phosphor of the image intensifier is lens coupled to a fast frame transfer cooled CCD camera.

II. ORIGINAL RUBY TS SYSTEM

The previous ruby TS system on MAST[1,2] was a single pulse system with 300 spatial points; 100 of these points were at high optical contrast (50% MTF). The majority of components of the previous system have been replaced to improve the spatial resolution and reduce the error of the electron temperature and density measurement. A recent upgrade to the Nd:YAG Thomson scattering system,[6] which shared the same collection optics as the original ruby system, required redesign of the F/12 collection lens to an F/6 collection lens. This new lens was incompatible with the original ruby system and thus provided an opportunity to upgrade it. Table I gives an estimated photon budget for the new and old core TS systems on MAST.

III. OPTICAL DESIGN

The design objectives of the upgraded system were to achieve the best possible radial resolution and to collect the largest number of scattered photons while effectively eliminating stray laser and plasma light. The system can be broken down into three major components, the collection lens, the optical fibers, and the spectrometer, and each will be discussed here.

TABLE I. Photon budget for new and existing MAST TS systems.

	New ruby	Original ruby	Nd:YAG
Resolution (mm)	7	15	10
F/#	15	15	6
Input slit width (mm)	8.5	7.5	N.A
Laser Energy (J)	10	10	1.6
EQE (%)	18	6.7	8–15
Transmission (%)	20	20	40
f_{detected}[a] (%)	90	90	60
p.e.[b] (/cm/10^{19})	3300	1100	2900

[a]Detected fraction of photoelectrons at 1 keV.
[b]Effective number of detected photoelectrons per centimeter of scattering length per 10^{19} m^{-3} of plasma density.

A. Collection lens and fiber bundles

The collection cell has six radiation tolerant lenses that withstand the effects of neutral beam generated neutrons. Four of these lenses are made from silica and the remaining two manufactured from radiation hardened flint glass. The collection cell has a diameter of 520 mm and a length of 650 mm. The combined weight of the collection cell and lenses is ~90 kg. Thomson scattered light is collected at F/6 from the 1.5 m Nd:YAG and ruby laser chord and imaged with a demagnification of 0.29 onto two F/1.75 fiber backplanes. The fibers used are plastic clad silica (PCS) and are not radiation resistant. Calculations based on the worst case neutron damage estimates predict a 10% to 15% reduction in transmission in the red part of the spectrum over the next ten years of MAST operation. These estimates are based on the published measurements[7,8] of the induced absorption of PCS fibers.

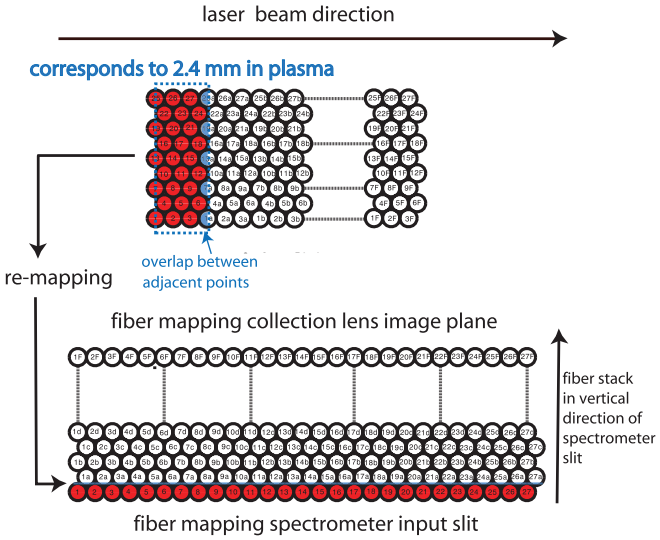

FIG. 2. (Color online) The mapping of the fiber bundles from the collection lens to the spectrometer input slit. The overlapping of fibers results in redistribution of light into the neighboring channels.

Downloaded 11 Aug 2011 to 194.81.223.66. Redistribution subject to AIP license or copyright; see http://rsi.aip.org/about/rights_and_permissions

Eighty-five coherent fiber bundles are used to map the image of the ruby laser chord to the input slit of the ruby spectrometer (see Fig. 2). Each of these fiber bundles is 12 m long and contains 243 fibers. The inner diameter of each fiber is 210 μm and the outer diameter, including cladding is 230 μm. The numerical aperture of each fiber is 0.37. The minimum size resolvable is determined by the mapping of the fiber bundles and for this system is 2.4 mm of the laser chord. The fibers are hexagonally packed to collect as much scattered light as possible from the fiber back plane. However, this close packing results in a redistribution of scattered light into the neighboring radial channels. At the collection lens the fiber packing results in a 9% redistribution of light into neighboring channels and a further 5% is redistributed at the spectrometer input slit (see Fig. 2).

The fiber bundle array is imaged onto the input slit by means of a relay lens system, which is based on a Petzval lens configuration (M = 1.5). Scattered light is collected from the fiber bundles at F/4 and telecentrically imaged onto two holographic notch filters. The notch filters are placed on the outer edges of the spectrometer slit. These filters remove the laser light at high optical density (6 O D) around a narrow 10 nm bandstop. At lower electron temperatures the narrow bandstop of these filters increases the detected fraction of the Thomson spectra by up to 20% for the 10–100 eV range (see Fig. 7).

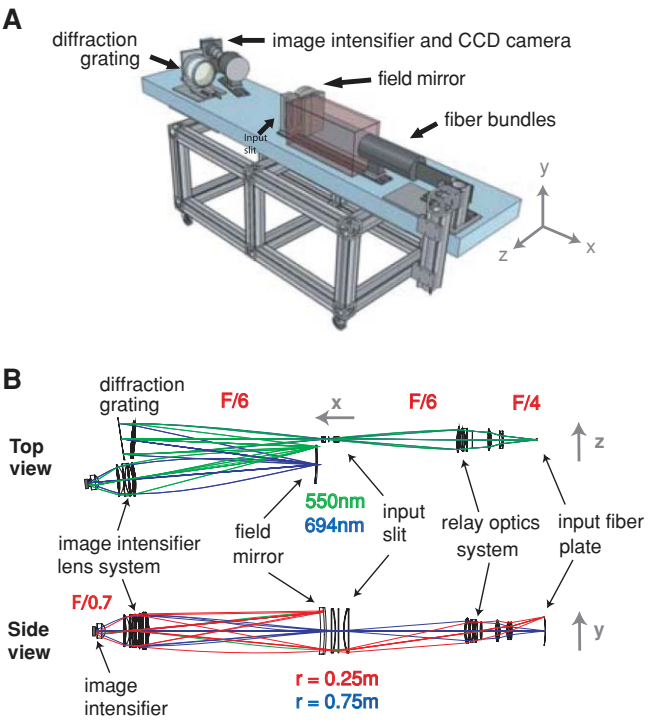

FIG. 3. (Color online) (a). The layout of the new spectrometer. (b). Two sets of optical rays are traced for two different wavelengths and two different radial positions. The rays form intermediate image planes at the input slit and field mirror before finally being imaged at the front of the image intensifier. Details of the CCD camera coupling lenses are not shown as these are commercial lenses and lens designs are not available.

B. Spectrometer

The spectrometer is based on a Littrow design. A 600 lines/mm grating is used with a singlet Littrow lens to disperse the light onto a field mirror (see Fig. 3). The center laser wavelength and the D-alpha (654 nm) wavelength are masked on this intermediate image plane. The bandstop of these masks is ~15 nm. This is set by the width of the input slit and the linear dispersion of the grating.

Light leaving the grating is imaged onto a 25 mm diameter image intensifier using an F/0.7 lens. The size of the image intensifier limits the etendue of the spectrograph and currently it is not possible to get a GEN 3 filmless image intensifier greater than 25 mm in diameter. An extremely low F-number is exploited to couple as much light as possible and a cylindrical lens is contact-mounted to the front of the image intensifier to correct for any aberrations across the field. The light is finally coupled to the CCD camera using two camera lenses with a demagnification of 0.37.

IV. SYSTEM PERFORMANCE

Extensive Monte Carlo modeling has been performed in the design of the upgraded ruby TS system and predicts how the system will perform. The fractional error in T_e and n_e as a function of T_e is shown in Fig. 4. The fractional error in T_e in the lower T_e range (<40 eV) increases as the Thomson spectra width approaches the bandstop of the Notch filters. The removal of the D-alpha wavelength results in a slight increase in the fractional error of T_e in the 80–200 eV range. The fractional error in n_e is determined by the photon statistics of the photo electrons detected once a minimum bandstop of the scattered spectrum can be detected.

One of the major factors that determines the error in the electron temperature and density measurement is the choice of the photocathode of the image intensifier. GaAsP photocathodes have higher quantum efficiency than GaAs, but their sensitivity goes toward zero beyond 800 nm. For the electron temperature range expected on MAST (0–5000 eV) the higher quantum efficiency of GaAsP photocathodes was found to be more important than the greater spectral range of GaAs photocathodes.

The major contributions to the background noise are brehmsstrahlung, line emission and the CCD noise. The amount of brehmsstrahlung is determined by the gate duration of the image intensifier and at 50 ns is typically very low. The ratio of scattered signal to brehmsstrahlung is very high as a result of the high energy of the ruby laser pulse. The effect of line emission is determined by plasma impurity conditions. Typically no line emission is observed in the ruby TS spectra. In the case of plasma start-up and low density measurement the ruby can be operated to measure the background light 230 μs after measurement of the Thomson spectra. The effect of the CCD noise is determined by the gain of the image intensifier and the coupling lens efficiency. If this is sufficiently high then the effect of the CCD noise is negligible. The CCD noise can be reduced further by binning pixels and reducing the number of spectral bins.

The very low background noise on this system (see Fig. 4) means that it can be used to measure the very low

Downloaded 11 Aug 2011 to 194.81.223.66. Redistribution subject to AIP license or copyright; see http://rsi.aip.org/about/rights_and_permissions

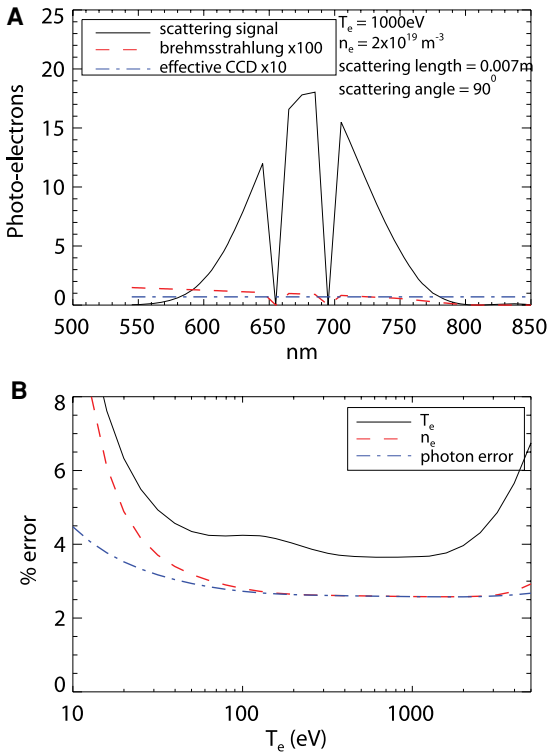

FIG. 4. (Color online) (A). Predicted TS spectra. The number of photo electrons is the number of detected photons evaluated at the image intensifier photo cathode. The noise is dominated by the Poisson noise of the scattered signal. The effective CCD amplitude is determined by dividing the square of the CCD read noise by the product of the image intensifier gain, CCD gain and the coupling lens efficiency (see Table II). B. The variation of the fractional T_e and n_e as a function of T_e. The photon error is the Poisson error of the number of scattered photons detected.

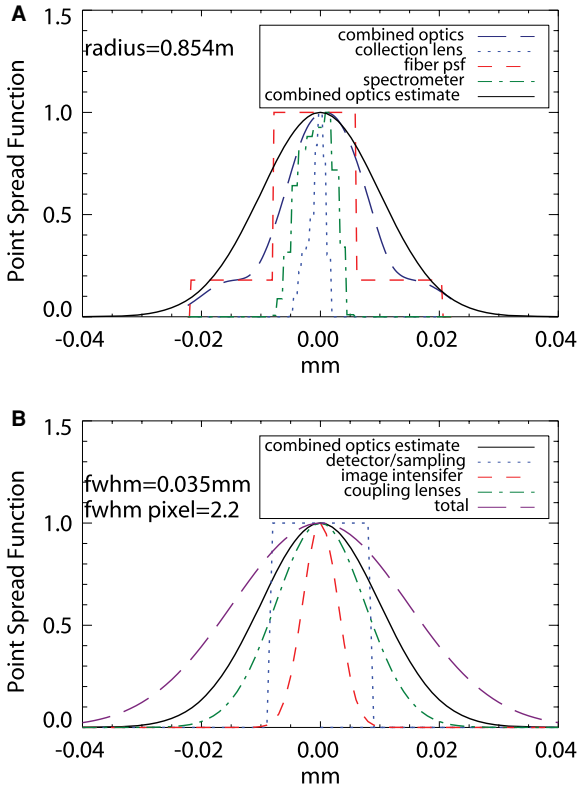

FIG. 5. (Color online) Contribution of different components to the spatial resolution of the ruby TS system evaluated on the CCD camera. (A). Contribution of components prior to the image intensifier. The PSF for the collection lens and spectrometer has been determined by tracing optical rays though each system for a radial location of 0.854 m. The combined optics PSF for the collection lens, spectrometer and fiber bundles is represented by a Gaussian of a full width half max (fwhm) of 0.024 m. (B). Contribution of components after the image intensifier to the final PSF of the entire system. This has a fwhm of 0.035 mm or 2.2 pixels.

electron densities that occur in plasma start-up experiments on MAST. The signal can even be binned to reduce the radial resolution and increase the number of photo electrons and hence reduce the error in electron temperature and density.

V. IMPROVED RESOLUTION

The spatial resolution achievable with the ruby TS system is determined by the convolution of the instrument function for each of the components that the scattered light passes through. Using optical ray tracing techniques it is possible to determine the instrument function of both the collection lens and the spectrometer system.

The contribution of the collection optics and spectrometer optics to the point spread function (PSF) can be estimated using field line tracing techniques. Estimates of these values determined using the optical design program ZEMAX are shown in Fig. 5(a). These PSF values are also convolved with a PSF that represents the distribution of light due to the fiber bundle mapping and the final result is a PSF representing all these contributions. This has been evaluated at different positions in the field of the lens system and is well represented by a Gaussian with a full width half max (fwhm) of 0.024 mm. This approximation has been used to represent the PSF of the collection lens, fiber bundles and spectrometer system prior to the image intensifier. This estimate is finally convolved with the PSF arising from the coupling lenses, image intensifier and CCD camera pixel size and sampling to give the final PSF of the entire system [see Fig. 5(b)] This has a fwhm of 0.035 mm which corresponds to 2.2 pixels or ~200 points resolved at 50% MTF.

The major limiting factor for the resolution is the combined optics PSF. After this, the component with the second biggest impact on the resolution is the coupling lens which couples light from the phosphor of the image intensifier to the CCD chip. For the upgraded system two commercial camera lenses were used; both focused at infinity. An F/2.8 zoom lens is reversed and attached to the front of an F/1 lens. The overall resolution is the combination of the resolution of each lens (~40 cycles/mm at 50% contrast). The resolution of this component and the system as a whole could be increased using a custom lens solution.

The PSF of the CCD camera is the combination of both the detector and sampling PSFs. The detector PSF is given by the width of the detector, which in this case is one pixel (16 μm). The sampling PSF arises because the position of the image with respect to the pixel position affects the final image resolution; distortion makes it impossible to align the CCD pixel perfectly with the object points. Following Park[9] a sampling PSF is defined where the sampling interval is the

Downloaded 11 Aug 2011 to 194.81.223.66. Redistribution subject to AIP license or copyright; see http://rsi.aip.org/about/rights_and_permissions

center-to-center spacing in the pixel array, which in case of this CCD chip is equal to the detector size.

VI. TRIGGERING

Plasma events are typically much faster than the repetition rate of a ruby laser. To gain the maximum possible information a "SMART" real time triggering unit has been developed separately[10] to trigger the ruby laser on specific plasma events, such as pellet injection and rotating magnetic islands. This unit triggers the ruby laser and a custom designed unit that controls how the image intensifier and CCD camera are triggered (see Fig. 6).

The image intensifier acts as a fast optical gate (50 ns). If the detector were not gated around the laser pulse, the plasma noise would be greater than the scattered light. A small fraction of the laser oscillator beam is used to trigger the image intensifier and a constant fraction discriminator (CFD) generates an electric pulse from this optical signal. The trigger point of this unit is largely independent of signal amplitude to eliminate any jitter of the image intensifier gate due to laser energy.

The CFD then triggers a complex programmable logic device (CPLD) based unit which has been programmed asynchronously in VHSIC hardware description language to generate the pulses required by the image intensifier gating unit. This unit can operate in two modes, the mode of operation being controlled by an optical trigger sent by the smart triggering unit.

In the first mode of operation, the laser is triggered once and one image of the Thomson scattered light and background light is taken. In the second mode of operation, the laser is triggered twice and two images of the Thomson scattered light are taken. It is critical that the CPLD unit operates as quickly as possible so that the image intensifier gate can be open and synchronized with the arrival of the scattered light. When this unit is programmed asynchronously the time delay between

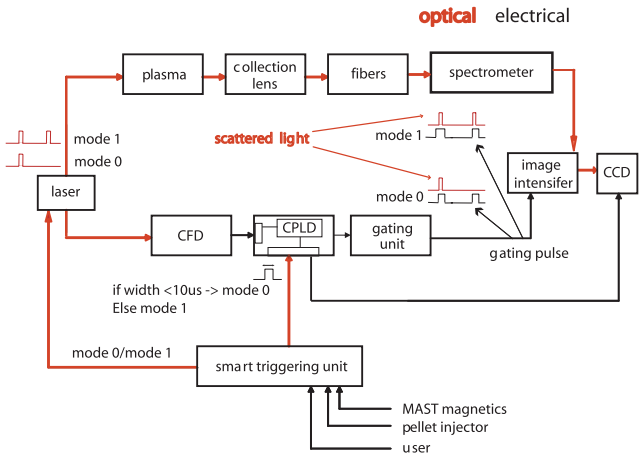

FIG. 6. (Color online) Triggering of the ruby TS system. The "SMART" trigger unit sends optical pulses to the laser and CPLD unit in either single pulse (mode 0) or double pulse (mode 1) operation. For double pulse operation the image intensifier opens in synchronisation with the ruby laser pulses. In single pulse operation the second image intensifier gate measures the plasma background radiation.

TABLE II. Efficiency of the detector system.

	New ruby	Old ruby
CCD Quantum Efficiency @550 nm	90%	70%
Image intensifier EQE	18	6
Spectral range of spectrometer[a]	550–800 nm	600–900 nm
efficiency of phosphor(photons/electrons)	21	70
CCD read noise (e^-rms)	3.5	4
CCD gain (counts/e^-)	1.5	0.5
Coupling efficiency of relay lenses	4%	4%
Counts/photo electron[b]	180	100

[a]The spectral range of the spectrometer is a combination of the spectral range of both the spectrometer and the image intensifier. The new GaAsP intensifier has a lower spectral range than the previous GaAs intensifier.
[b]The number of counts/photo electron is given by the product of the image intensifier photon gain (G_p), the efficiency of the coupling lenses (ϵ) and the CCD camera gain and Q.E.

the rising edge input and output pulses can be reduced to 14 ns. By comparison, the fastest off-the-shelf pulse generator surveyed introduced a time delay of 50–80 ns. Such an off-the-shelf solution would also have increased hardware costs by a factor of 10.

VII. DETECTOR SYSTEM

The scattered light is detected using an image intensifier lens coupled to a cooled CCD camera. Specifically, a GaAsP filmless image intensifier is coupled to a back-illuminated fast frame transfer CCD camera. Each component of this detection system is discussed in the following sections and the parameters which determine the efficiency of the system are shown in Table II.

A. Image intensifier

A Hamamatsu filmless GaAsP 25 mm diameter Gen 3 image intensifier was found to be most suitable for the ruby upgrade requirements. The photocathode has a peak quantum efficiency (QE) of 35%. The peak effective quantum efficiency (EQE $= QE/(N_f)^2$) is ~18% over the spectral range (550–800 nm) of the spectrometer. N_f is the noise factor, which is the ratio of the input and output signal to noise ratio and represents additional losses in the image intensifier. A P46 phosphor with a decay time of 0.2 μs is used to allow two images to be taken in quick succession. The photon gain (G_p) of the image intensifier is given by

$$G_p = QE \times G_c \times P_e, \quad (1)$$

where G_c is the electron gain of the micro channel plate (MCP) (500–1000) and P_e is the conversion factor of input electrons to photons at the phosphor (~21 photons/electrons). The maximum achievable gain is ~8000 at the peak MCP voltage.

B. CCD camera

The CCD camera is a cooled PRO EM camera from Princeton instruments. This camera uses a back-illuminated

Downloaded 11 Aug 2011 to 194.81.223.66. Redistribution subject to AIP license or copyright; see http://rsi.aip.org/about/rights_and_permissions

CCD and has ~90% QE between 550–700 nm, which is well matched to the output spectrum of the phosphor. It has two readout amplifiers, a slow (100 kHz) low noise amplifier which is currently being used and a 10 MHz electron multiplication amplifier, which could be used for future high repetition measurements of T_e and n_e profiles.

The CCD chip has an array of 512 × 1040 square pixels; each pixel is 16 μm × 16 μm. The camera is used in frame transfer mode, where 512 × 512 pixels (8.2 mm × 8.2 mm) are active and the remaining pixels are used for storage. The read noise at 100 kHz is 3.5 electrons rms and the vertical transfer time is 450 ns per row. The minimum time required to transfer a 512 × 512 image into the storage region is 230 μs. Thus two images can be captured separated by 230 μs; the second image recorded will either be the plasma background light or a second snapshot of the T_e and n_e profile. The time between captured images is well matched to the optimum separation required to double pulse the ruby laser.

C. Coupling lenses

The coupling efficiency (ϵ) between the image intensifier and the CCD camera is determined by the ratio of the solid angle collected to the solid angle emitted by the phosphor, multiplied by a transmission coefficient of the optics (T). CCD cameras can be coupled to image intensifiers using fiber stubs or lenses. Although coupling efficiency is typically greater for fiber stubs, less flexibility exists in terms of magnification (m), CCD camera choice and area of image intensifier utilized. For these reasons lens coupling was chosen for this application. The coupling efficiency of a perfect lens illuminated by a Lambertian source[11] is given by

$$\epsilon = \frac{T}{4F^2(m+1)^2}, \tag{2}$$

where F is the F number of the lens system, calculated from the ratio of the limiting aperture diameter to the focal length of the lens system. For this system a Canon 80–150 mm F2.8 zoom lens is coupled to a Canon 50 mm F/1 lens. The first lens acts as a collimator and converges the divergent light from the phosphor into a parallel beam. The second lens focuses the light onto the CCD camera. The demagnification (m) for these lenses is adjusted to 0.37 to match the area of the CCD camera. The coupling efficiency of this system is ~4%, which is greater than expected from Eq. (2) because the phosphor screen produces more forward directed light than a Lambertian source.

At the edge of the field, optical vignetting reduces the coupling efficiency to ~1%. The reduction of optical coupling at the edge of the field is a result of the relative separation of each lens stop. The low CCD read noise and the high photon gain of the system allow acceptable signal to noise at the edges of the image. These edges correspond to the edges of the MAST plasma.

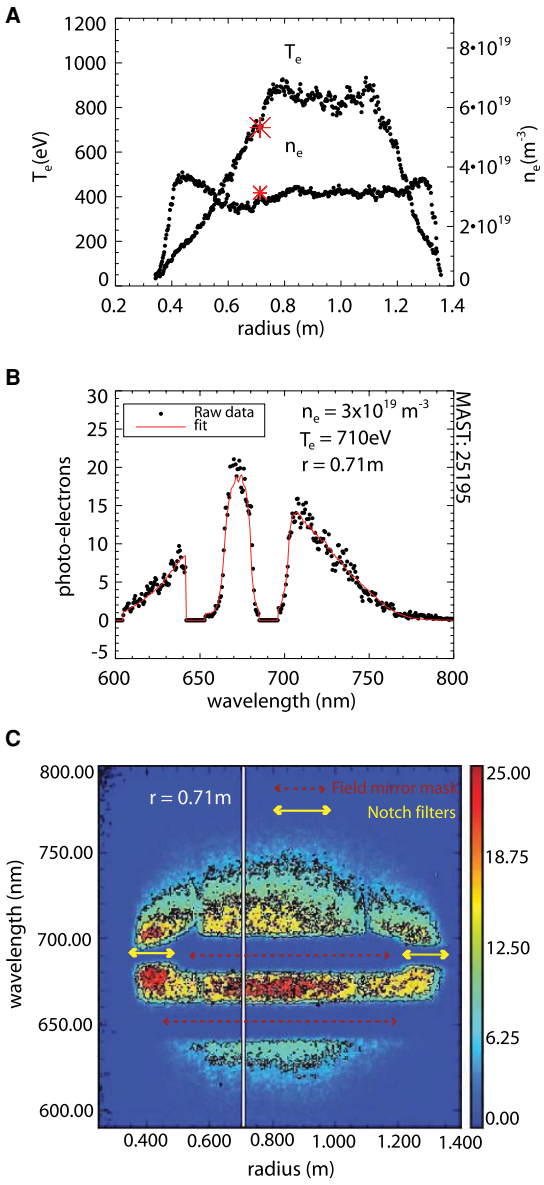

FIG. 7. (Color online) (A). Electron temperature and density profiles for a typical MAST shot. B. The fitted spectrum corresponds to the radial position of the star in A. C. The photoelectrons recorded by the CCD camera. Notch filters at the edge of the image remove less of the scattered signal around the laser wavelength than the field mirror mask used for the hot central region.

VIII. RESULTS

The first results from the system were obtained in September 2009. Figure 7(a) shows 512 point profiles of electron temperature and density. A fit to the spectra at one radial point is shown in Fig. 7(b) and Fig. 7(c) shows the number of scattered photo electrons detected by the system as a function of radius and wavelength.

IX. NOISE STATISTICS

For CCD based ruby TS systems, the noise statistics detected (C_{pe}) are determined by two factors, the number of scattered photons (S_{pe}) and the convolution of the PSF ($I(k,l)$), of the image intensifier and coupling lenses[12]

Downloaded 11 Aug 2011 to 194.81.223.66. Redistribution subject to AIP license or copyright; see http://rsi.aip.org/about/rights_and_permissions

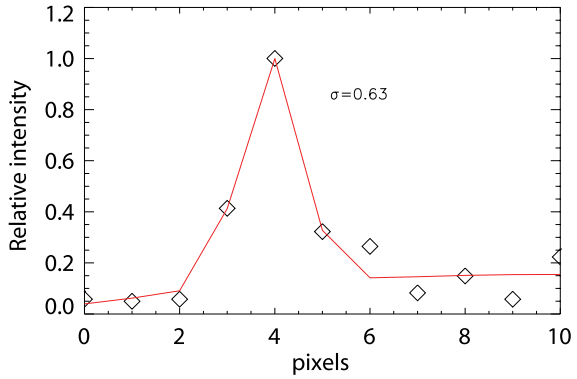

FIG. 8. (Color online) PSF of the image intensifier and coupling lenses. This smooths the noise before it is measured by the CCD.

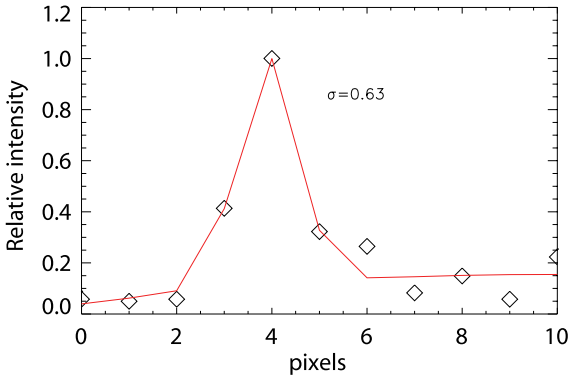

FIG. 9. (Color online) The theoretical and measured number of photo electrons detected by the ruby TS system. The number of detected photo electrons has been determined from the variance of the noise from a white-light source. The read noise from the CCD camera is 0.03 photo electrons per pixel.

$$C_{pe}(i, j) = \sum_k \sum_l S_{pe}(i-k, j-l) I(k, l). \quad (3)$$

This PSF smooths the noise before it is measured by the CCD camera. The PSF itself is measured by operating the system in photon counting mode and measuring the PSF detected from a single photon incident on the photo cathode (see Fig. 8). The variance of the noise detected (σ_{Cpe}) is given by the convolution of the square of the smoothing PSF and the photon noise on the photo cathode,

$$\sigma^2_{Cpe}(i, j) = \sum_k \sum_l \sigma^2_{pe}(i-k, j-l) I^2(k, l). \quad (4)$$

It is assumed the amplitude of scattered photons does not change significantly over the width of the PSF,

$$\sigma^2_{Cpe}(i, j) = \sigma^2_{pe}(i-k, j-l) \sum_k \sum_l I^2(k, l), \quad (5)$$

$$= \sigma^2_{pe}(i-k, j-l) \Gamma_{pe,i} \quad (6)$$

where $\Gamma_{\mathrm{pe,i}}$ is the reduction factor for the noise and is the total sum of the square of the 2D PSF smoothing function. This is calculated to be a factor of 4.4, assuming a symmetric smoothing function. Once the smoothing PSF is known, the number of photo electrons can be determined by measurement of the variance of the noise of the system.

A calibrated white light source has been used to determine the noise statistics of the upgraded TS system. This lamp is used to illuminate a Lambertian diffuser which is placed in front of the collection lens. The noise has been calculated by determining the variance of the signal over a large number of pixels and is dominated by the photon statistics of the detected photo electrons. A good agreement is found between the theoretical performance determined using the parameters in Tables I, II and the noise measured (see Fig. 9).

X. SUMMARY AND FUTURE PROSPECTS

A new TVTS system has been built that can resolve 200 points at high contrast along a 1.4 m chord. The system can measure two images separated by 230 μs, which can be exploited to measure two electron temperature and density profiles or one electron temperature and density profile with the background light. The detection elements of this system have been designed to allow for future multi pulse operation with a higher repetition rate ruby laser. The design of the collection lens and fiber bundles allows for future increase in optical throughput by a factor of 4, although a major redesign of the spectrometer would be required.

In this paper the contribution of each component to the spatial resolution has been modeled and the final performance of the system agrees well with this model. The components which have been found to limit the system are the fiber bundles, the relay lens system and the CCD detector, and sampling PSFs.

ACKNOWLEDGMENTS

This work was funded by the United Kingdom Engineering and Physical Sciences Research Council under Grant EP/G003955 and the European Communities under the contract of Association between EURATOM and CCFE. The views and opinions expressed herein do not necessarily reflect those of the European Commission. The authors are indebted to their colleagues in the drawing office, especially Phil Parsons. Data acquisition would have been impossible without the help of Nigel Thomas Davies.

[1] M. J. Walsh, E. R. Arends, P. G. Carolan, M. R. Dunstan, M. J. Forrest, S. K. Nielsen, and R. O'Gorman, Rev. Sci. Instrum. **74**, 1663 (2003).
[2] M. Walsh, N. J. Conway, M. Dunstan, M. Forrest, and R. B. Huxford, Rev. Sci. Instrum. **70**, 742 (1999).
[3] D. Johnson, N. Bretz, D. Dimock, B. Grek, D. Long, R. Palladino, and E. Tolnas, Rev. Sci. Instrum. **57**, 1856 (1986).
[4] C. J. Barth, H. J. v. d. Meiden, T. Oyevaar, and N. J. Lopes Cardozo, Rev. Sci. Instrum. **72**, 1138 (2001).
[5] H. J. van der Meiden, C. J. Barth, T. Oyevaar, S. K. Varshney, A. J. H. Donné, M. Yu. Kantor, D. V. Kouprienko, A. Alexeev, W. Bie, and A. Pospieszczyk, Rev. Sci. Instrum. **75**, 3849 (2004).
[6] R. Scannell, M. J. Walsh, P. G. Carolan, M. Dunstan, R. B. Huxford, G. McArdle, D. Morgan, G. Naylor, T. O'Gorman, S. Shivbaev, and M. J. Walsh, Rev. Sci. Instrum. **79**, 10E730-2 (2008).
[7] G. H. Sigel, E. J. Friebele, M. E. Gingerich, and L. M. Hayden, IEEE Trans. Nucl. Sci. **26**, 4796 (1979).
[8] A. T. Ramsey, H. G. Adler, and K. W. Hill, Internal PPPL Report, 1995.
[9] S. K. Park, R. Schowengerdt, and M. Kaczynski, Appl. Opt. **23**, 2572 (1984).
[10] G. Naylor, Fusion Eng. Des. **85**, 280 (2010).
[11] A. D. A. Maidmenty, and M. J. Yaffe, Phy. Med. Biol. **41**, 475 (1996).
[12] M. N. A. Beurskens, C. J. Barth, C. C. Chu, and N. J. Lopes, Rev. Sci. Instrum. **70**, 1999 (1999).

Downloaded 11 Aug 2011 to 194.81.223.66. Redistribution subject to AIP license or copyright; see http://rsi.aip.org/about/rights_and_permissions